Electronic Supplementary Material

Central core size effect in quinoxaline-based non-fullerene acceptors for high V_{OC} organic solar cells

Xinya Ran,[a,b] Yanan Shi,[a] Dingding Qiu,[a,b] Jianqi Zhang,[a] Kun Lu,*[a,b] Zhixiang Wei [a,b]

[a] CAS Key Laboratory of Nanosystem and Hierarchical Fabrication, National Center for Nanoscience and Technology, Beijing 100190, China

[b] Sino-Danish Center for Education and Research, Sino-Danish College, University of Chinese Academy of Sciences, Beijing 100049, China

E-mail: lvk@nanoctr.cn

1. Synthesis of Qx-BO-1，Qx-BO-2，Qx-BO-3.
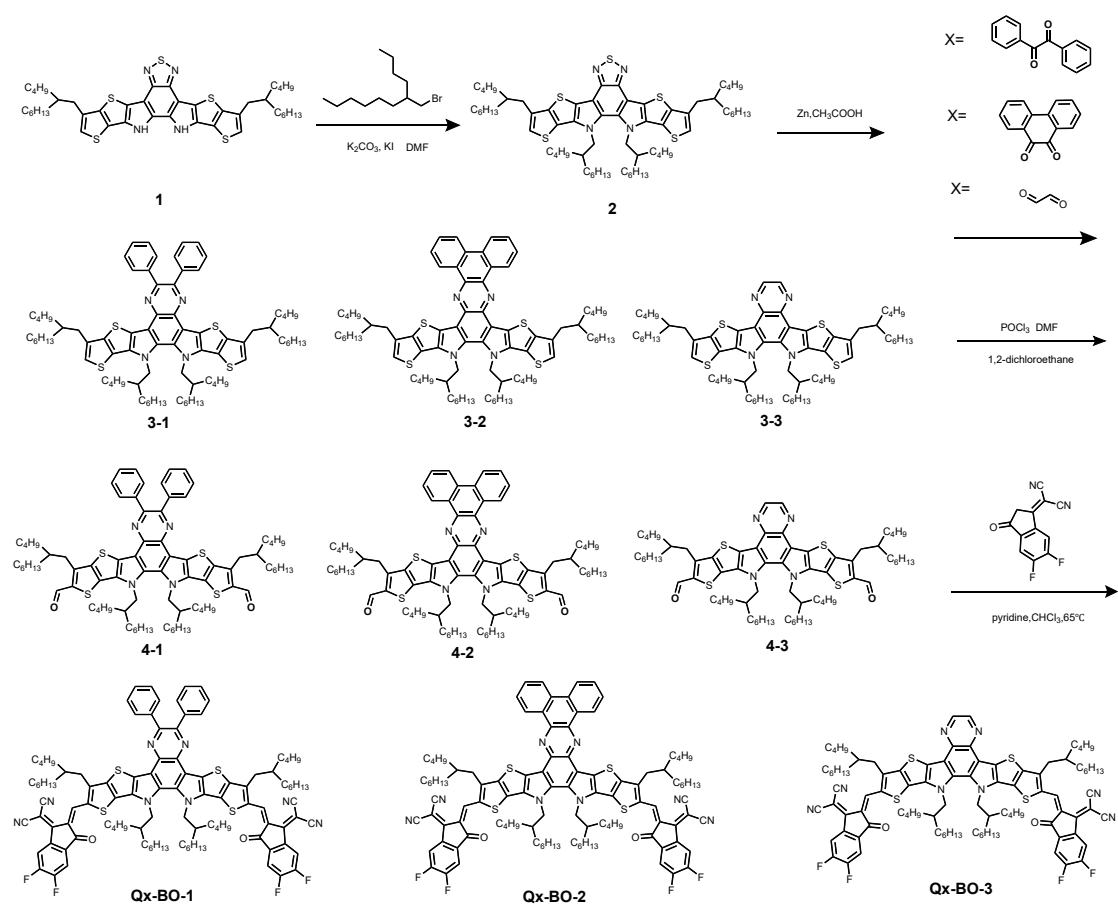
Scheme S1 Synthetic routes of Qx-BO-1, Qx-BO-2 and Qx-BO-3

The chemical name of materials:

Qx-BO-1:2,2'-((2Z,2'Z)-((3,10,13,14-tetrakis(2-butyloctyl)-6,7-diphenyl-13,14-dihydrothieno[2'',3'':4',5']thieno[2',3':4,5]pyrrolo[3,2f]thieno[2'',3'':4',5']thieno[2',3':4,5]pyrrolo[2,3-h] quinoxaline-2,11-diyl)bis(methaneylylidene))bis(5,6-difluoro-3-oxo-2,3-dihydro-1H-indene-2,1-diylidene))dimalononitrile.

Qx-BO-2: 2,2'-((2Z,2'Z)-((7,10,11,14-tetrakis(2-butyloctyl)-10,11-dihydrodibenzo [a,c]thieno [2'',3'':4',5']thieno[2',3':4,5]pyrrolo[3,2-h]thieno[2'',3'':4',5']thieno[2',3':4,5] pyrrolo[2,3-j] phenazine-8,13-diyl)bis(methaneylylidene))bis(5,6-difluoro-3-oxo-2,3-dihydro-1H-indene-2,1-diylidene))dimalononitrile.

Qx-BO-3:2,2'-((2Z,2'Z)-((3,10,13,14-tetrakis(2-butyloctyl)-13,14-dihydrothieno [2'',3'':4',5'] thieno[2',3':4,5]pyrrolo[3,2-f]thieno[2'',3'':4',5']thieno [2',3':4,5]pyrrolo [2,3-h]quinoxaline-2,11-diyl)bis(methaneylylidene))bis(5,6-difluoro-3-oxo-2,3-dihydro-1H-indene-2,1-diylidene)) dimalononitrile.

Compound2:3,9,12,13-tetrakis(2-butyloctyl)-12,13-dihydro-[1,2,5]thiadiazolo[3,4e] thieno[2'',3'':4', 5']thieno[2',3':4,5]pyrrolo[3,2-g]thieno[2',3':4,5]thieno[3,2-b]indole.

Compound 3-1：3,10,13,14-tetrakis(2-butyloctyl)-6,7-diphenyl-13,14-dihydrothieno [2'', 3 ' ':4',5']thieno[2',3':4,5] pyrrolo[3,2-f]thieno[2'',3'':4',5']thieno [2',3':4,5] pyrrolo [2,3-h] quino-xaline.

Compound 3-2:7,10,11,14-tetrakis(2-butyloctyl)-10,11-dihydrodibenzo[a,c]thieno [2'',3'':4',5'] thieno[2',3':4,5]pyrrolo[3,2-h]thieno[2'',3'':4',5']thieno [2',3':4,5] pyrrolo [2,3-j]phenazine.

Compound 3-3:3,10,13,14-tetrakis(2-butyloctyl)-13,14 dihydrothieno[2'',3'':4',5'] thieno [2 ',3':4,5]pyrrolo[3,2-f]thieno[2'',3'':4',5']thieno[2',3':4,5]pyrrolo[2,3 h] quinoxaline

Compound 4-1: 3,10,13,14-tetrakis(2-butyloctyl)-6,7-diphenyl-13,14 dihydrothieno [2'', 3'':4',5'] thieno[2',3':4,5]pyrrolo[3,2-f]thieno[2'',3'':4',5']thieno[2',3':4,5]pyrrolo [2,3 h]quino- xaline-2,11-dicarbaldehyde.

Compound 4-2: 7,10,11,14-tetrakis(2-butyloctyl)-10,11-dihydrodibenzo[a,c]thieno[2 ", 3":4',5'] thieno[2',3':4,5]pyrrolo[3,2-h]thieno[2",3":4',5']thieno[2',3':4,5]pyrrolo[2,3-j]phen azine-8,13-dicarbaldehyde.

Compound 4-3: 3,10,13,14-tetrakis(2-butyloctyl)-13,14-dihydrothieno [2",3":4',5'] thieno [2 ',3':4,5]pyrrolo[3,2-f]thieno[2",3":4',5']thieno[2',3':4,5]pyrrolo[2,3-h] quinoxaline-2,11-dicarbaldehyde.

Compound 2: Compound 1 (600mg, 0.77mmol), K_2CO_3 (1064.14mg, 7.7mmol), KI (1278.2mg, 7.7mmol) and 50mlDMF were dissolved in a 100ml three-necked flask, flushed with N_2 three times, and heated to 80°C. 5-(bromomethyl) undecane (1919.14mg, 7.7mmol) was weighed by subtraction and added into a three-neck flask, heated to 95°C, and reacted overnight. After cooling to room temperature, the solvent was removed under reduced pressure, extracted with saturated brine and dichloromethane, and dried. The crude product was then purified by silica-gel column chromatography to obtain compound 2 as an orange solid. (300mg, 50% yield). ^{1}H NMR (300 MHz, CDCl$_3$,) δ6.97 (s, 2H), 4.57-4.55 (d, J = 7.5 Hz 4H), 2.76-2.73 (d, J = 7.3 Hz 4H), 2.06-2.00 (m, 4H), 1.38-0.93 (m, 64H), 0.65-0.59 (m, 24H).

Compound 3-1：To a solution of compound 2(300mg, 0.28mmol) in acetic acid (50 mL) was added zinc powder (728mg, 11.2mmol) in one portion. Then the mixture solution was heated to 90°C for 5 h. After the solution was cooled at room temperature, the solid was removed by filtration. Transfer the filtrate to a three-tip flask containing 5-(bromomethyl) undecane (171.3mg, 0.81mmol), then the mixture solution was heated to 110°C for 20 h. After cooling to room temperature, washed with saturated salt water and methylene chloride. The solvent was removed under reduced pressure. The crude product was subsequently purified by column chromatography on silica gel to afford compound 3-1 as yellow oily solid (100mg, 30% yield).^{1}H NMR (400 MHz, CDCl$_3$) δ 7.76 (d, J = 6.4 Hz, 4H), 7.33-7.28 (m, 6H), 6.99 (s, 2H), 4.59 (d, J = 7.7 Hz, 4H), 2.75 (d, J = 7.2 Hz, 4H), 2.12-2.04 (m, 4H), 1.35 – 0.58 (m, 88H).

Compound 3-2: Compound 3-2 was synthesized by similar procedure as compound 3-

1 between compound 2 and compound phenanthrene-9,10-dione. The final product was obtained as yellow solid (100mg, 30% yield). ^{1}H NMR (400 MHz, CDCl$_3$) δ 9.75 (d, J = 8.0 Hz, 2H), 8.71 (d, J = 8.0 Hz, 2H), 7.87 (dd, J = 25.5, 7.0 Hz, 4H), 7.01 (d, J = 9.8 Hz, 2H), 4.71 (s, 4H), 3.21 (d, J = 8.0 Hz, 4H), 2.01 (d, J = 5.9 Hz, 4H), 1.43-0.94 (m, 64H), 0.92-0.66 (m, 24H).

Compound 3-3：Compound 3-2 was synthesized by similar procedure as compound 3-1 between compound 2 and compound Glyoxal. The final product was obtained as yellow solid (150mg, 50% yield).^{1}H NMR (400 MHz, CDCl$_3$) δ 8.92 (s, 2H), 7.05 (s, 2H), 4.59 (m, 4H), 2.86 (t, J = 7.6 Hz, 4H), 2.05 (m, 4H), 1.50-1.11 (m, 64H), 1.02-0.60 (m, 24H).

Compound 4-1: Compounds 3-1 (100 mg; 0.08mmol) were dissolved into 1,2-dichloroethane (20 ml) in a three-neck flask. The solution was flushed with nitrogen in 0°C for 30 min. Then, add POCl3 (0.25 mL) and DMF (0.25 mL) to the solution, then let the solution temperature return to room temperature for 1h. Next, the solution was reacted at 85 °C for 16 h under nitrogen protection. After that the mixture was poured into ice water (50 mL), neutralized with aqueous AcONa. Washed with saturated salt water and dichloromethane. The solvent was removed under reduced pressure. The crude product was subsequently purified by column chromatography on silica gel to afford compound 4-1 as orange solid (86mg, 90% yield). ^{1}H NMR (400 MHz, CDCl$_3$) δ 10.18 (s, 2H), 7.86-7.81 (m, 4H), 7.49-7.44 (m, 6H), 4.72 (t, J = 11.5 Hz, 4H), 3.24 (t, J = 7.6 Hz, 4H), 2.01-1.91 (m, 4H), 1.45-0.92 (m, 64H), 0.86-0.64 (m, 24H).

Compound 4-2: Compound 4-2 was synthesized by similar procedure as compound 4-1 with compound 3-2. The final product was obtained as orange solid (84mg, 90% yield). ^{1}H NMR (400 MHz, CDCl$_3$) δ 10.22 (s, 2H), 9.70 (dd, J = 7.8, 1.1 Hz, 2H), 8.68 (d, J = 8.0 Hz, 4H), 7.96 (ddd, J = 15.2, 11.4, 4.3 Hz, 4H), 4.77 (d, J = 7.9 Hz, 4H), 3.33 (t, J = 7.6 Hz, 4H), 2.09-1.97 (m, 4H), 1.53 – 0.93 (m, 64H), 0.84-0.56 (m, 24H).

Compound 4-3: Compound 4-3 was synthesized by similar procedure as compound 4-1 with compound 3-3. The final product was obtained as orange solid (180mg, 90%

yield). ^{1}H NMR (400 MHz, CDCl$_3$) δ 10.17 (s, 2H), 8.94 (s, 2H), 4.72 (m, 4H), 3.22 (t, J = 7.6 Hz, 4H), 2.07-1.99 (m, 4H), 1.50 -1.12 (m, 64H), 1.08-0.65 (m, 24H).

Qx-BO-1: INCN-2F (164mg, 0.7 mmol) and compound 4-1 (86 mg, 0.07 mmol) were added to a solvent mixture of chloroform (20 mL). After 0.8mL pyridine were added, the mixture was stirred at 65°C overnight. After cooling to room temperature, the reaction mixture was poured into water and extracted several times with chloroform. Removed solvent by reduced pressure and the residue was purified on a silica-gel column chromatography using chloroform as eluent to give Qx-BO-1 as blue solid. (110mg, 90%yield)^{1}H NMR (400 MHz, CDCl$_3$) δ 9.15 (s, 1H), 8.58 (m, 2H), 7.79 (dd, J = 6.6, 2.9 Hz, 4H), 7.70 (t, J = 7.5 Hz, 2H), 7.48-7.40 (m, 6H), 4.82 (d, J = 7.8 Hz, 4H), 3.21 (d, J = 7.3 Hz, 4H), 2.21 (s, 2H), 2.08 (s, 2H), 1.50-0.97(m, 64H), 0.90-0.83(m, 12H), 0.71-0.67(m, 12H). MALDI-TOF MS (m/z): 1736.813. Elemental analysis: calculated for C$_{106}$H$_{116}$F$_4$N$_8$O$_2$S$_4$ (%): C, 73.24; H, 6.73; N, 6.45; S, 7.38 Found (%):C, 73.25; H, 6.75; N, 6.46; S, 7.36

Qx-BO-2: Compound Qx-BO-2 was synthesized by similar procedure as Qx-1 between compound 4-2 and INCN-2F. The final product was obtained as black solid (100mg, 85% yield).^{1}H NMR (400 MHz, CDCl$_3$) δ 9.58-9.56 (m, 2H), 9.08 (s, 2H), 8.73-8.71 (m, 2H), 8.35 (s, 2H), 7.90 (dd, J = 6.0, 3.1 Hz, 4H), 7.59 (t, J = 7.3 Hz, 2H), 4.90 (d, J = 7.5 Hz, 4H), 3.24 (d, J = 5.7 Hz, 4H), 2.35-2.14 (m, 4H), 1.45-0.97(m, 64H), 0.98 - 0.64(m, 24H). MALDI-TOF MS (m/z): 1734.792. Elemental analysis: calculated for C$_{106}$H$_{114}$F$_4$N$_8$O$_2$S$_4$ (%): C, 73.32; H, 6.62; N, 6.45; S, 7.39 Found (%):C, 73.19; H, 6.61; N, 6.30; S, 7.33

Qx-BO-3: Compound Qx-BO-3 was synthesized by similar procedure as Qx-1 between compound 4-3 and INCN-2F. The final product was obtained as blue solid (210mg, 85% yield).^{1}H NMR (400 MHz, CDCl$_3$) δ 9.16 (s, 2H), 8.99 (s, 2H), 8.57 (dd, J = 9.9, 6.5 Hz, 2H), 7.70 (t, J = 7.5 Hz, 2H), 4.81 (d, J = 7.8 Hz, 4H), 3.21 (d, J = 7.6 Hz, 4H). 2.18-2.11 (m, 4H), 1.47-1.25 (m, 64H), 0.87-0.80 (m, 12H), 0.72-0.65 (m, 12H). MALDI-TOF MS (m/z): 1584.797. Elemental analysis: calculated for C$_{94}$H$_{108}$F$_4$N$_8$O$_2$S$_4$ (%): C, 71.18; H, 6.86; N, 7.06; S, 8.08 Found (%):C, 71.18; H, 6.91; N, 7.04; S, 8.06

2. Experimental

Materials and synthesis

Solvents and other common reagents were obtained from Beijing Chemical Plant. All other chemicals were purchased from commercial sources (Alfa, Acros, TCI, J&K, and Sigma–Aldrich) and used without further purification unless otherwise stated. PM6 was purchased from Solarmer Materials Inc. The detailed synthetic procedures of Qx-B0-1, Qx-BO-2 and Qx-B0-3 and the corresponding structural characterizations can be found in the Supplementary information.

Device fabrication

The OSCs devices were fabricated with conventional device structure of ITO/PEDOT:PSS/active layer/PNDIT-F3N/Ag. The PEDOT:PSS solution was spin coated on top of the cleaned ITO-coated glass substrate and the PEDOT:PSS film thickness was approximately 30 nm. After thermal annealing for 15 minutes at 150 °C. The blended solution was prepared by mixing donors and acceptor in a weight ratio into chloroform (CF) with the addition of a small amount of 1,8-diiodooctane. Subsequently, the active layer was spin-coated from blend chloroform solutions with a rotation speed in 3000-3500 r/min. After thermal annealing at 100°C for 10 min, a concentration of 0.5 mg/ml PNDIT-F3N with a small amount of acetic acid spin-coated on the active layer with a rotation speed of 3000 r/min. Finally, a layer of ~100 nm Ag layer was evaporated under a high vacuum ($<1 \times 10^{-4}$ Pa).

Measurements and instruments

Mass spectra were determined on a Bruker microflex MALDI-TOF mass spectrometer. ^{1}H NMR was obtained on a Bruker Avance 400 NMR spectrometer using tetramethylsilane as an internal standard. The geometry structures of three acceptors were optimized by using DFT calculations (B3LYP/6-31G(d, p)) and

all calculations were carried out using Gaussian 09. Ultraviolet-visible (UV−vis) spectra was obtained with a Perkin Elmer Lambda 950 spectrophotometer. Electrochemical cyclic voltammetry was conducted on a CHI 760E workstation with Pt plate coated with the small molecule film, Pt plate, and Ag/Ag$^+$ electrode as the working electrode, counter electrode, and reference electrode, respectively, in a 0.1 mol/L tetrabutylammonium hexafluorophosphate (Bu$_4$NPF$_6$) acetonitrile solution. Ag/Ag$^+$ electrode potentials were calibrated with the ferrocene/ferrocenium (Fc/Fc$^+$) redox couple (−4.8 eV relative to the vacuum level). Contact angle (θ) in solutions of PM6, Qx-BO-1, Qx-BO-2 and Qx-BO-3 are measured on ITO/glass substrate by using the pendant drop method with the XG-CAMB3 standard contact angle meter. The calculation of surface tension by DCA (dynamic contact angle). The Flory-Huggins interaction parameter can be written as the formula below:

$$\chi_{ij} = K\left(\sqrt{\gamma_i} - \sqrt{\gamma_j}\right)$$

Where K is a positive constant, where γ_i and γ_j are the surface energy of the donor and acceptor materials, respectively. The current density–voltage (J–V) characteristics were collected using a Keithley 2400 Source under an AM 1.5G spectrum from a solar simulator. Light intensity is calibrated with a Newport Oriel PN 91150V Si -based solar cell. The effective area of the device is 0.04 cm^2. The EQE measurements of the devices were performed in air with an Oriel Newport system (Model 66902) equipped with a standard Si diode. Monochromatic light was generated from a Newport 300 W lamp source. The thickness of the active layer was measured on a Kla-TencorAlpha-StepD-120 Stylus Profiler. EQE$_{EL}$ measurements were performed by applying external voltage/current sources through the devices (ELCT-3010, Enlitech). The electron mobility was acquired with the device structure of Al/Active layer /PNDIT-F3N-Br/Al, the hole mobility was obtained by preparing the structure of ITO/PEDOT:PSS/active layer/MoO$_x$/Ag. J–V characteristics were measured in

the range of 0-5 V using a Keithley 2400source-measure unit in the dark. For the fitting, an SCLC model was used mathematically expressed as:

$$J = \frac{9}{8}\varepsilon_0\varepsilon_r\mu_0\frac{(V - V_{bi})^2}{L^3}exp(0.89\gamma\sqrt{\frac{V - V_{bi}}{L}})$$

Where ε_0, ε_r is the dielectric constant of the semiconductor layer, μ_0 is the zero-field mobility, V_{bi} is the built-in potential due to the anode-cathode work function offset, L is the thickness of the active layer, and γ is the field-dependence coefficient. EQE_{EL} measurements were performed by applying external voltage/current sources through the devices (ELCT-3010, Enlitech). The E_{loss} in organic solar cells can be divided into three parts as follows:

$$E_{loss} = E_g^{pv} - qV_{OC}$$

$$= \left(E_g^{pv} - qV_{OC}^{SQ}\right) + \left(qV_{OC}^{SQ} - qV_{OC}^{rad}\right) + (qV_{OC}^{rad} - qV_{OC})$$

$$= \left(E_g^{pv} - qV_{OC}^{SQ}\right) + qV_{OC}^{rad, below\ gap} + qV_{OC}^{non-rad}$$

$$= q\Delta V_1 + q\Delta V_2 + q\Delta V_3$$

$$= \Delta E_1 + \Delta E_2 + \Delta E_3$$

In this formula, q is the elementary charge; $V^{SQ}\ OC$ is the maximum voltage in the Shockley–Queisser (SQ) limit model, and $V^{rad}\ OC$ is the open-circuit voltage with only radiative recombination in the device. Transmission electron microscopy (TEM) images were acquired on Tecnai G2 F20 U-TWIN TEM instrument. The atomic force microscopy (AFM) characterization was performed by Bruker Multimode 8 in Scan Asyst Mode in air. Grazing incidence wide angle X-ray scattering (GIWAXs) measurement was conducted at the beamline of 7.3.3 at the Advanced Light Source (ALS).
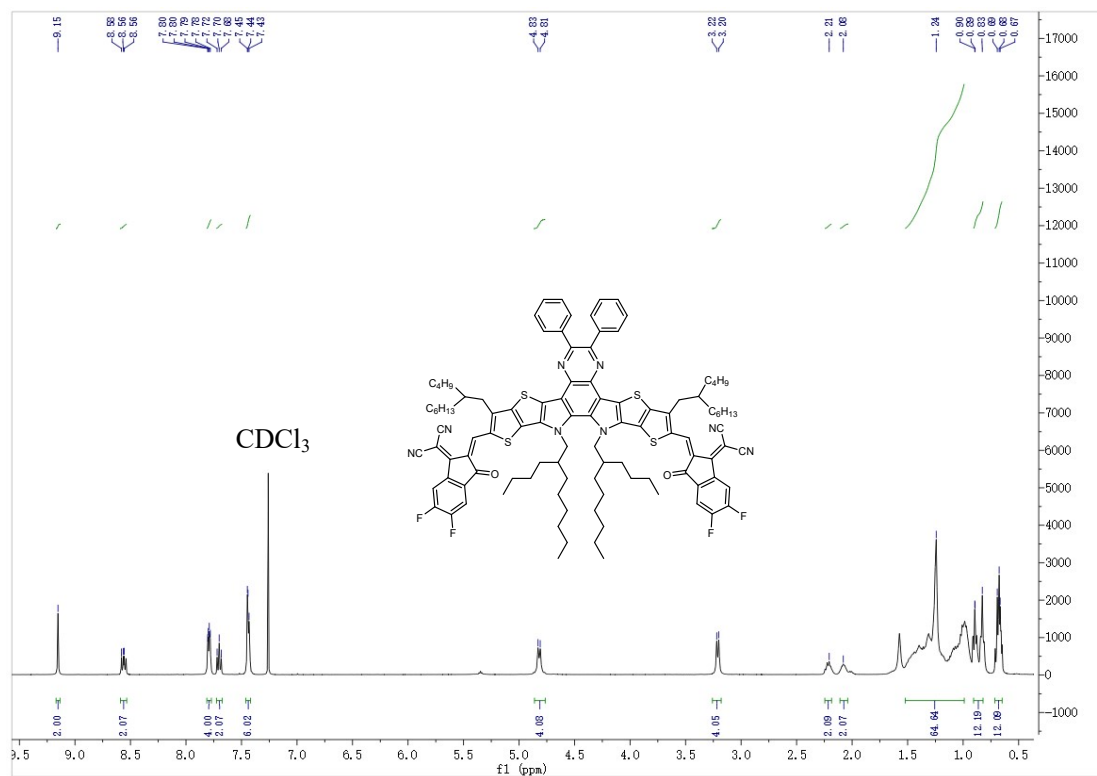
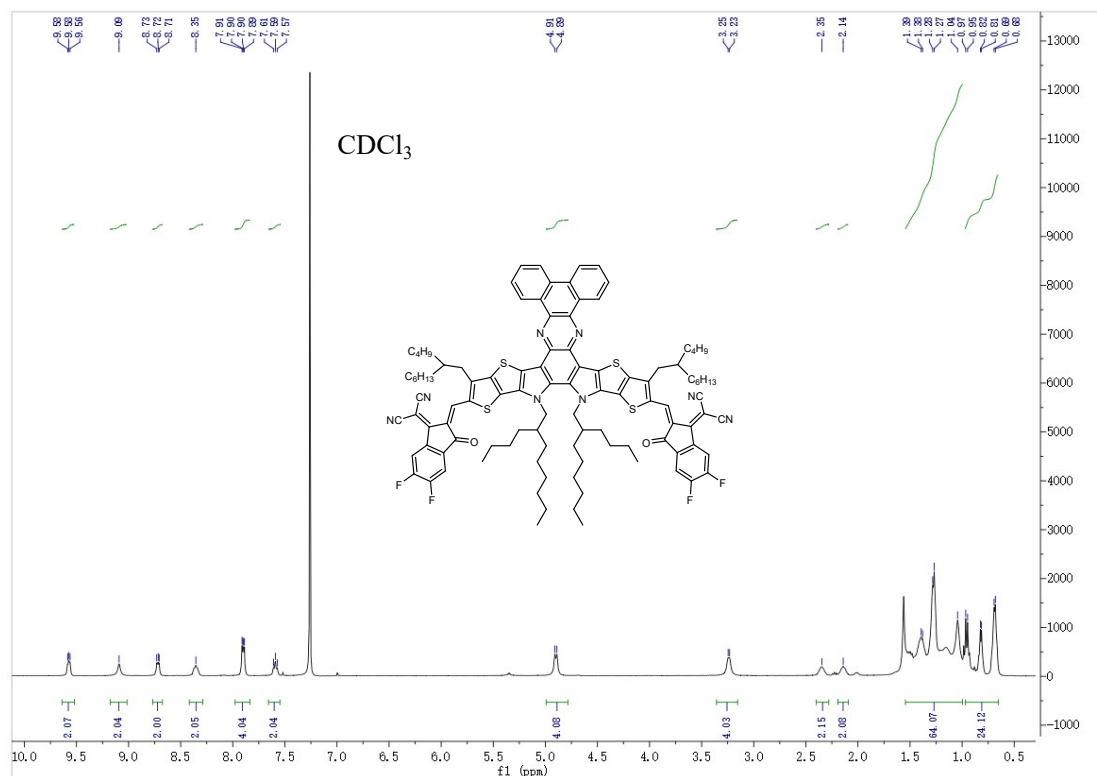# 3. Figures

Figure S1 ^{1}H NMR spectrum for Qx-BO-1.
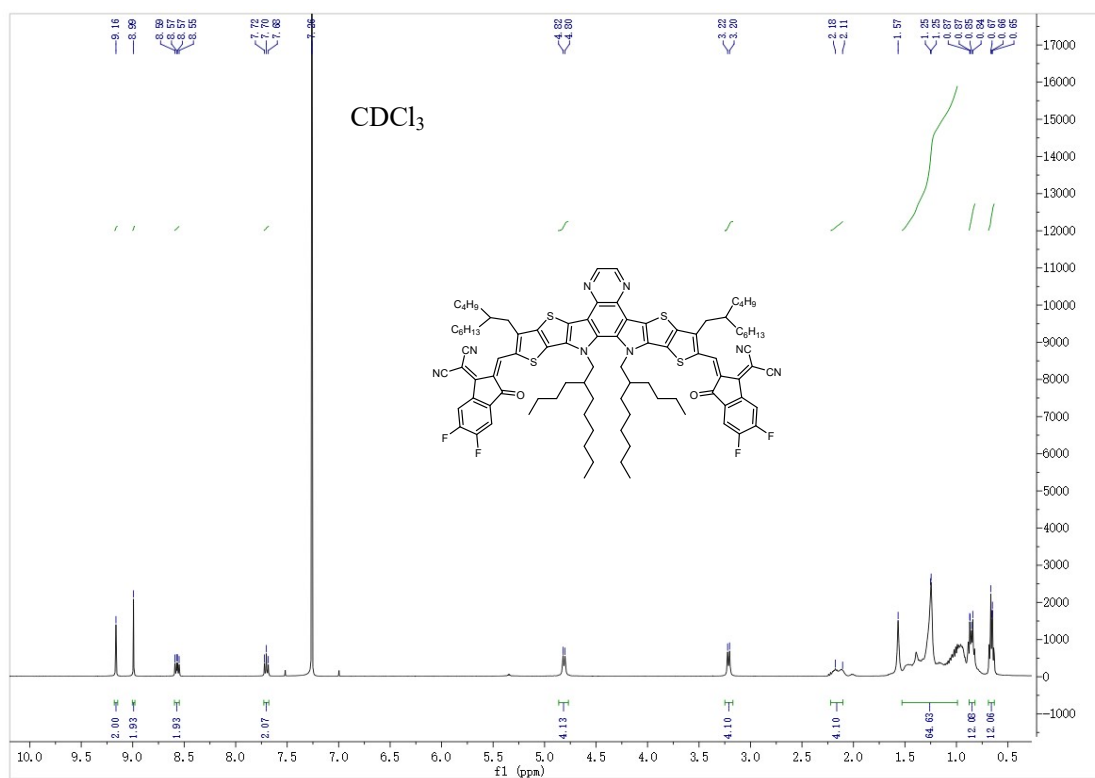

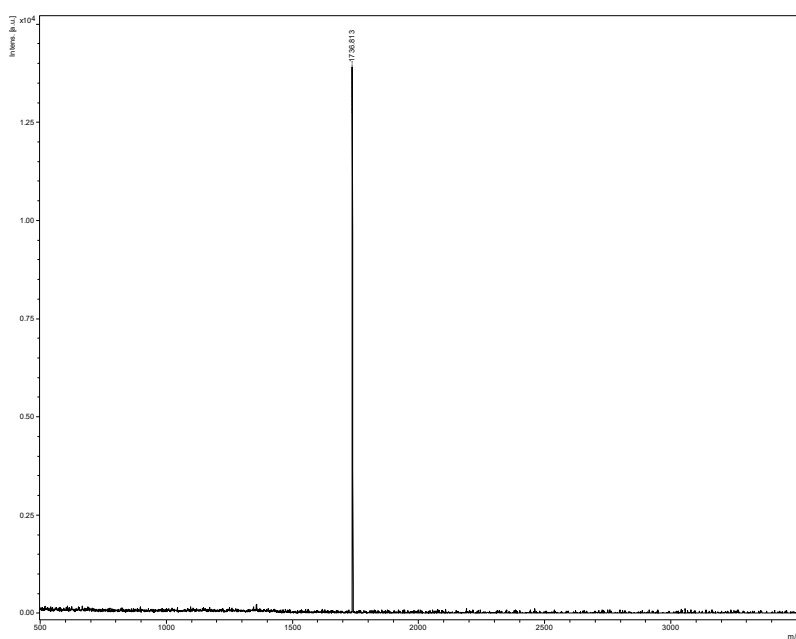**Figure S2** ^{1}H NMR spectrum for Qx-BO-2.

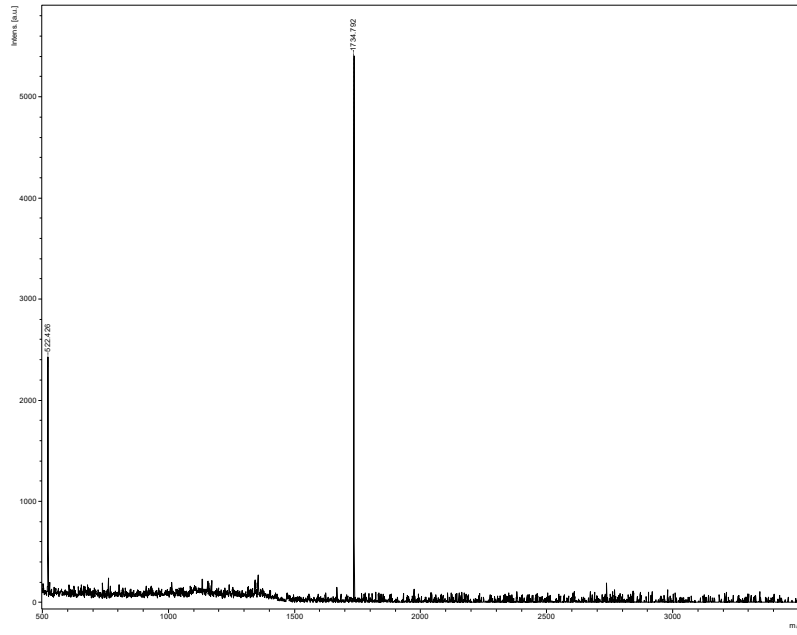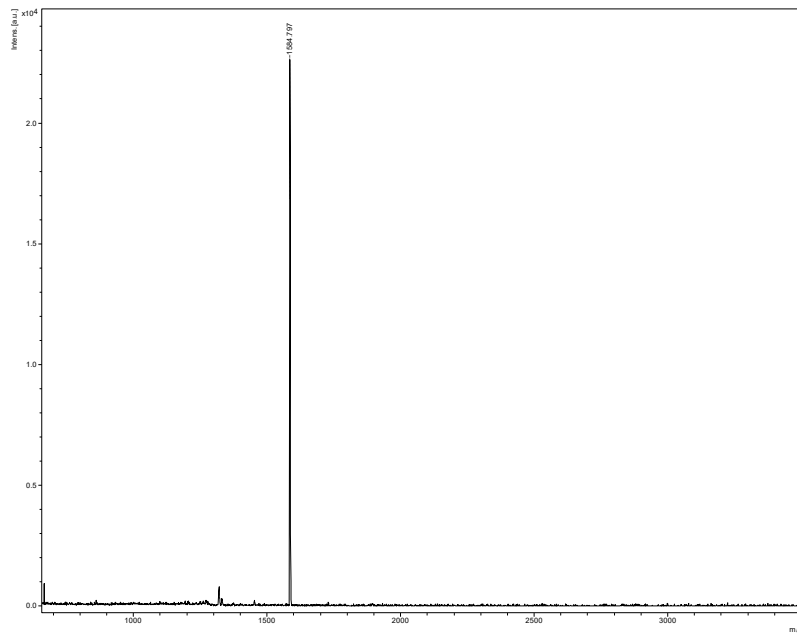**Figure S3** ^{1}H NMR spectrum for Qx-BO-3.

Figure S4 MALIDI-TOF mass spectrum of Qx-BO-1.

Figure S5 MALIDI-TOF mass spectrum of Qx-BO-2.

Figure S6 MALIDI-TOF mass spectrum of Qx-BO-3.
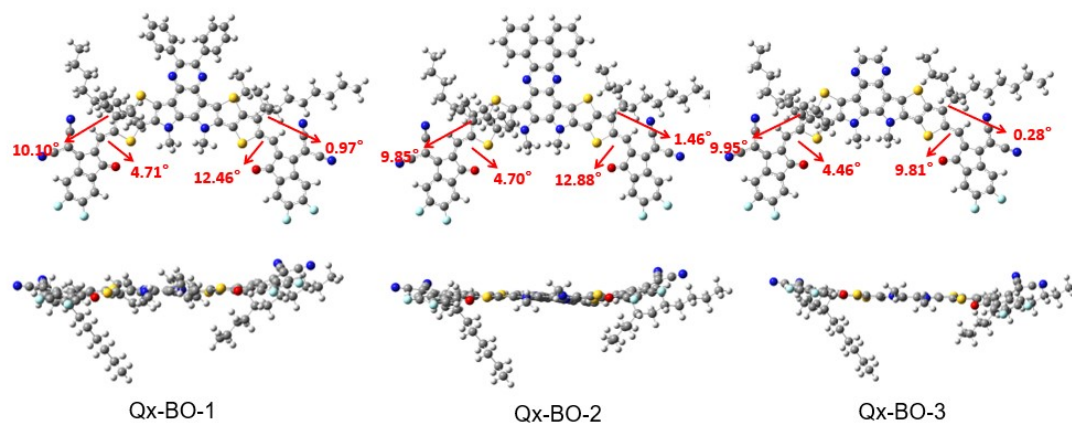
Figure S7 Optimal conformation simulated by DFT calculations for Qx-BO-1, Qx-BO-2 and Qx-BO-3 in simplified modes (top view and side view).
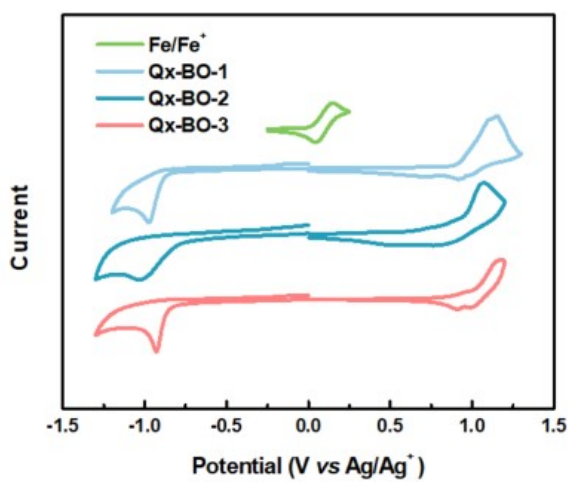
Figure S8 Cyclic voltammogram for the three acceptors.
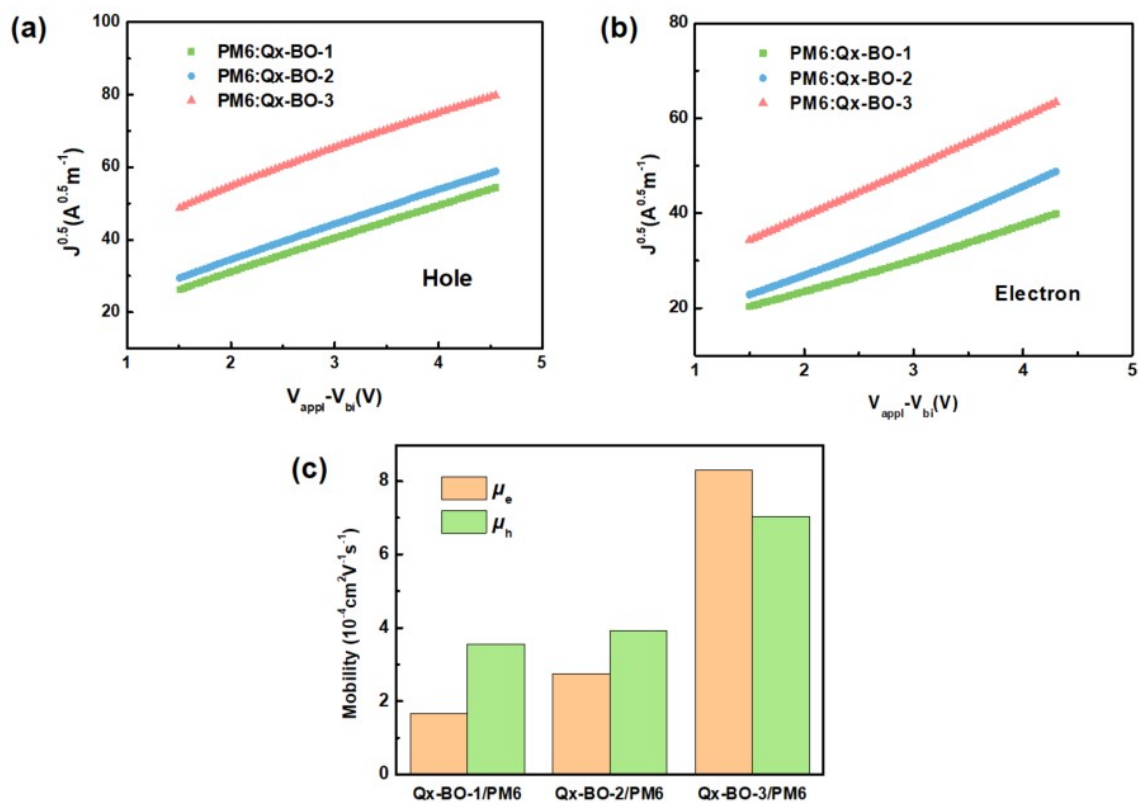
Figure S9 $J^{0.5} \sim V$ characteristics of the charge carrier mobility measurements of devices.
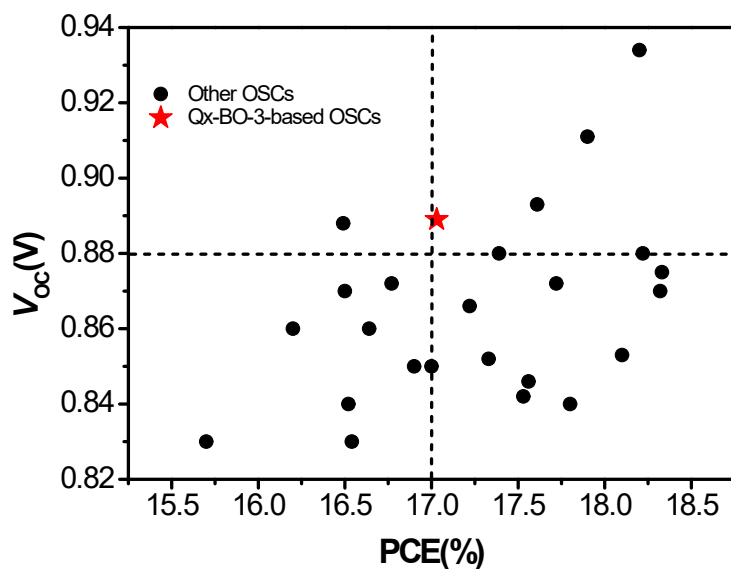
Figure S10. Plots of the PCE against V_{OC} for various systems based on Y-series derivatives.
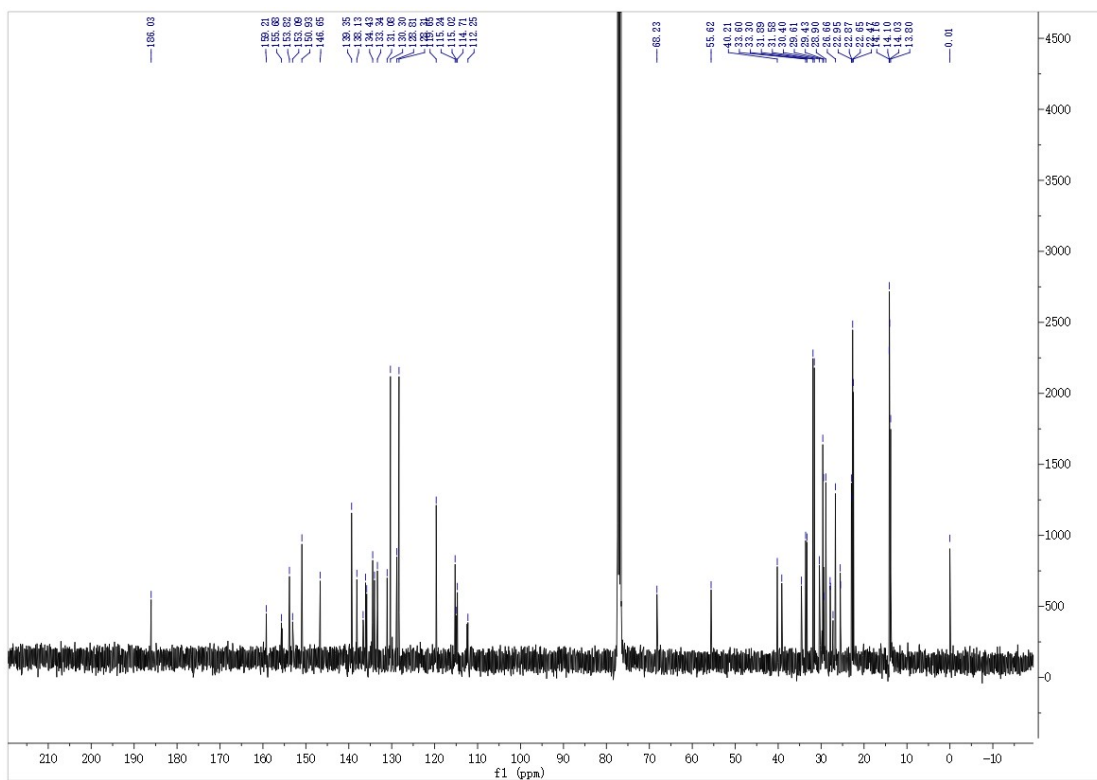
Figure S11. ^{13}C-NMR spectrum for Qx-BO-1.
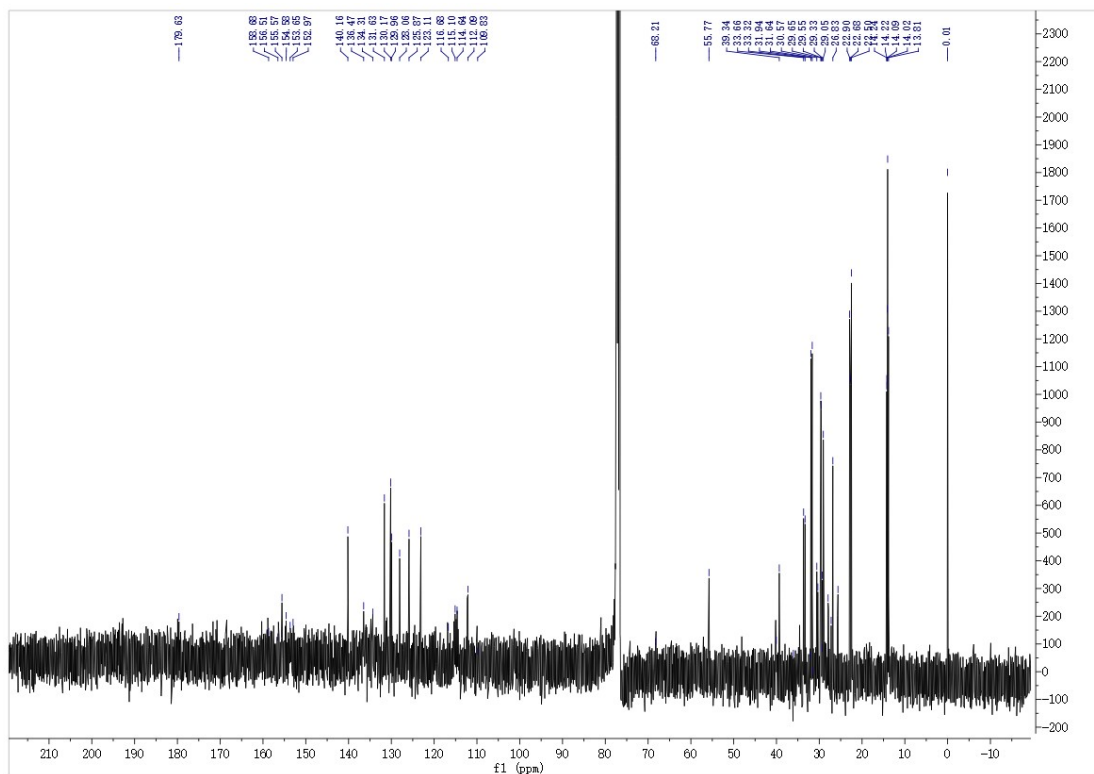
Figure S12. ^{13}C-NMR spectrum for Qx-BO-2.

Figure S13. ^{13}C-NMR spectrum for Qx-BO-3.
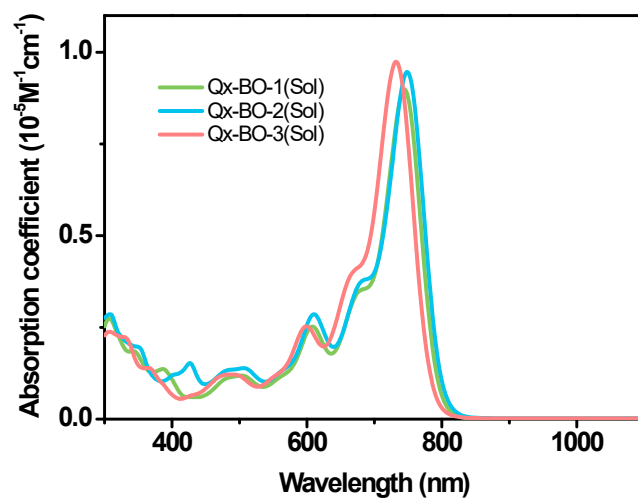
Figure S14. Solution absorption coefficient of Qx-BO-1, Qx-BO-2 and Qx-BO-3.
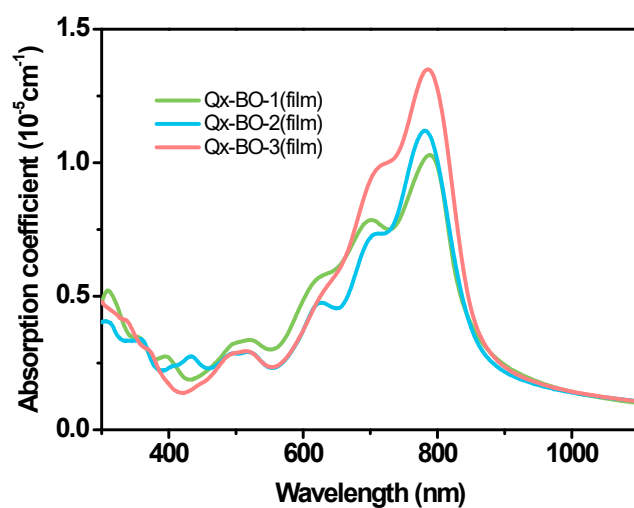
Figure S15. Film absorption coefficient of Qx-BO-1, Qx-BO-2 and Qx-BO-3.
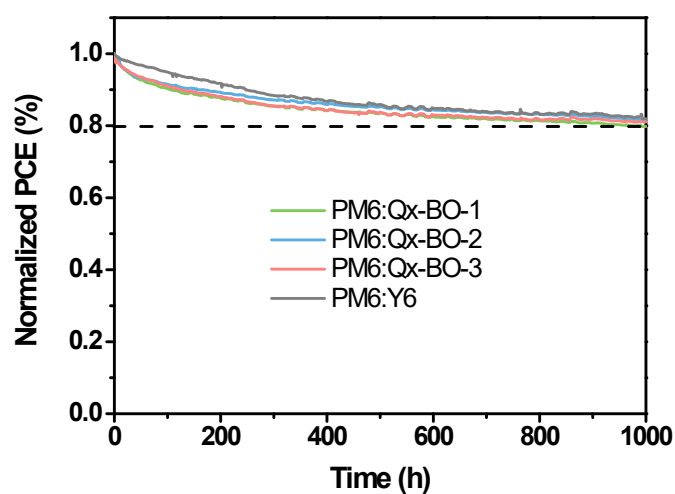
Figure S16. Photostability of PM6:Qx-BO-1, PM6:Qx-BO-2, PM6:Qx-BO-3 and PM6:Y6 based devices.

4. Tables

Table S1 Optical parameters and energy levels of Qx-BO-1, Qx-BO-2 and Qx-BO-3

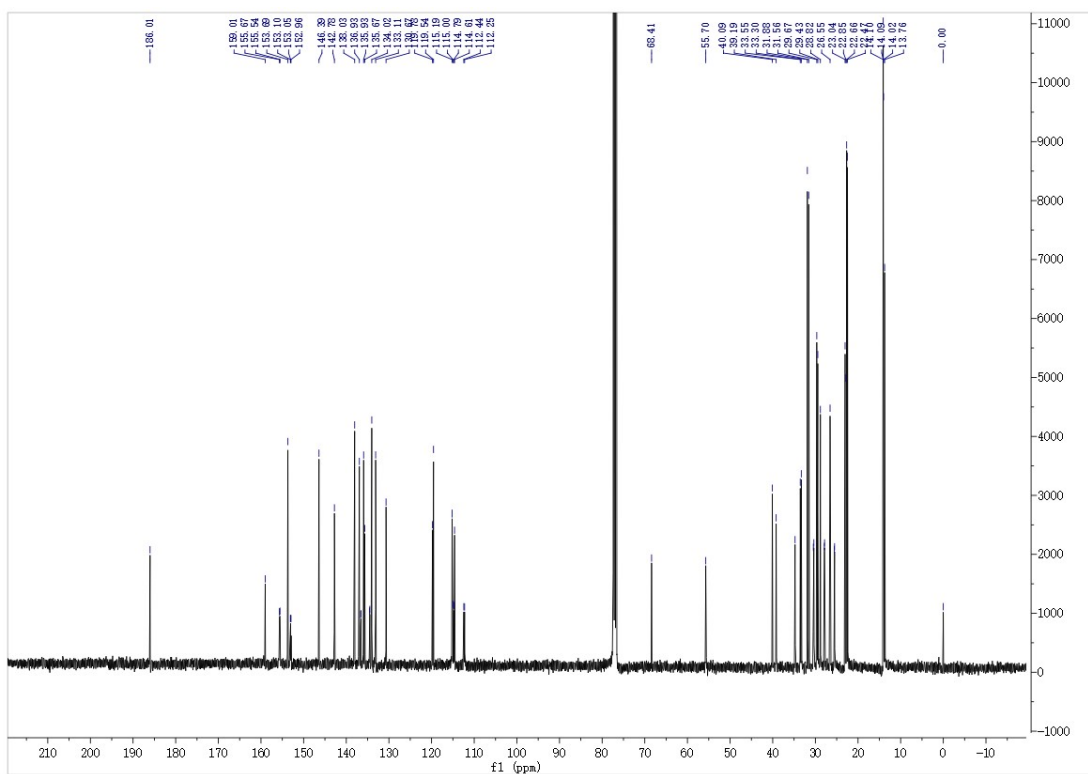| Acceptors	λ_{max}(nm) solution	λ_{max}(nm) film	λ_{onset}(nm) film	Eopt g (eV)	E_{HOMO} (eV)	E_{LUMO} (eV)	$E_{HOMO-cal}$ (eV)	$E_{LUMO-cal}$ (eV)
Qx-BO-1	745	786	847	1.46	-5.56	-3.74	-5.49	-3.65
Qx-BO-2	749	775	842	1.47	-5.50	-3.80	-5.50	-3.67
Qx-BO-3	733	791	881	1.41	-5.64	-3.84	-5.55	-3.78

Table S2 Device optimization for PM6: Qx-BO-1 blends.

D: A	Additives	Thermal annealing	V_{OC} (V)	J_{SC} (mA·cm^{-2})	FF (%)	PCE (%)
1:1	0.50% CN	100°C, 10 min	0.912	17.14	47.64	7.45
1:1.3	0.50% CN	100°C, 10 min	0.953	17.51	57.60	9.61
1:1.5	0.50% CN	100°C, 10 min	0.953	18.49	59.96	10.04
1:1.5	0.25% DIO	100°C, 10 min	0.969	12.59	58.17	7.09
1:1.5	0.60% CN	100°C, 10 min	0.936	18.63	58.66	10.23
1:1.5	0.30% CN	110°C, 10 min	0.951	17.49	62.22	10.35
1:1.5	0.30% CN	90°C, 10 min	0.955	18.11	58.97	10.20
1:1.5	0.30% CN	100°C, 10 min	0. 956	18.21	60.64	10.57

Table S3 Device optimization for PM6: Qx-BO-2 blends.

D: A	Additives	Thermal annealing	V_{OC} (V)	J_{SC} (mA·cm^{-2})	FF (%)	PCE (%)
1:1	0.50% CN	100°C, 10 min	0.956	19.07	59.39	10.83
1:1.2	0.50% CN	100°C, 10 min	0.960	18.96	60.99	11.11
1:1.3	0.50% CN	100°C, 10 min	0.959	19.14	61.31	11.26
1:1.3	0.25% DIO	100°C, 10 min	0.960	18.57	61.43	10.96
1:1.3	0.60% CN	100°C, 10 min	0.942	18.50	63.33	11.04
1:1.3	0.30% CN	110°C, 10 min	0.953	18.92	61.79	11.14
1:1.3	0.30% CN	90°C, 10 min	0.961	19.00	60.35	11.03
1:1.3	0.30% CN	100°C, 10 min	0. 963	19.18	61.49	11.34

Table S4 Device optimization for PM6: Qx-BO-3 blends.

D: A	Additives	Thermal annealing	V_{OC} (V)	J_{SC} (mA·cm^{-2})	FF (%)	PCE (%)
1:1	0.25% DIO	100°C, 10 min	0.879	24.26	75.79	16.15
1:1.2	0.25% DIO	100°C, 10 min	0.888	24.49	75.54	16.42
1:1.3	0.25% DIO	100°C, 10 min	0.878	24.49	75.75	16.28
1:1.4	0.25% DIO	100°C, 10 min	0.871	24.49	73.80	15.74
1:1.2	0.30% DIO	100°C, 10 min	0.893	24.48	76.83	16.80
1:1.2	0.35% DIO	100°C, 10 min	0.879	24.553	75.036	16.18
1:1.2	0.40% DIO	100°C, 10 min	0.861	24.437	74.155	15.61
1:1.2	0.50% CN	100°C, 10 min	0.873	23.22	76.11	15.42
1:1.2	0.60% CN	100°C, 10 min	0.868	23.09	74.98	15.02
1:1.2	0.30% DIO	90°C, 10 min	0.883	25.08	76.66	16.98
1:1.2	0.30% DIO	110°C, 10 min	0.889	24.76	77.39	17.03

Table S5 Charge carrier transport parameters of the optimized devices.

Diveces	$J_{ph(a)}$ (mA cm^{-2})	$J_{ph(b)}$ (mA cm^{-2})	J_{sat} (mA cm^{-2})	η_{diss} (%)	η_{coll} (%)
PM6: Qx-BO-1	21.16	19.26	21.63	97.83	89.04
PM6: Qx-BO-2	21.58	19.53	21.99	98.13	88.81
PM6: Qx-BO-1	25.73	24.97	25.80	99.72	96.78

(a The photocurrent density obtained under the maximum output power of the device)

(b The photocurrent density obtained under the short-circuit state of the device)

Table S6 The electron mobilities (μ_e)/hole mobilities (μ_h) value of the blend films

Active layer	μ_h(cm^2·V^{-1}·s^{-1})	μ_e(cm^2·V^{-1}·s^{-1})	μ_h/μ_e
PM6:Qx-BO-1	3.56×10-4	1.67×10-4	2.13
PM6:Qx-BO-2	3.92×10-4	2.75×10-4	1.42
PM6:Qx-BO-3	7.04×10-4	8.31×10-4	0.85

Table S7 Detailed E_{loss} of the devices.

Devices	$E_{pv}\,g$ (eV)	EQE_{EL}	$qV\text{S}Q_{OC}$ (eV)	$qV\text{rad}_{OC}$ (eV)	E_{loss} (eV)	ΔE_1 (eV)	ΔE_2 (eV)	ΔE_3 (eV)
PM6: Qx-BO-1	1.484	6.85×10-4	1.218	1.162	0.503	0.266	0.048	0.189
PM6: Qx-BO-2	1.480	7.58×10-4	1.213	1.159	0.507	0.267	0.054	0.186
PM6: Qx-BO-3	1.456	1.42×10-4	1.192	1.135	0.550	0.264	0.057	0.229

Table S8 The parameters of surface energies.

Acceptors	$\gamma^{accepter}$ (mN/m^2)	Donor	γ^{donor} (mN/m^2)	χ/ K(γD^{-2}-γA^{-2})^2
QX-BO-1	15.98	PM6	11.82	0.31
QX-BO-2	15.35	PM6	11.82	0.23
QX-BO-3	14.81	PM6	11.82	0.17

Table S9 GIWAXS measurement parameters of the related films

Films		q (Å^{-1})	d-spacing (Å)	FWHM (Å^{-1})	CCL (Å)
Qx-BO-1		1.70	3.70	0.158	39.77
Qx-BO-2	OOP (010)	1.70	3.70	0.184	34.15
Qx-BO-3		1.73	3.63	0.455	13.81
PM6: Qx-BO-1		1.65	3.81	0.279	22.52
PM6: Qx-BO-2	OOP (010)	1.79	3.51	0.242	25.96
PM6: Qx-BO-3		1.69	3.72	0.407	15.44

Table S10 Device parameters for high performance OSCs in the literature.

Acceptor	Donor	V_{oc} (V)	PCE (%)	FF	J_{sc} (mA cm^{-2})	Ref. (SI)
Y6	PM6	0.83	15.7	0.75	25.3	[1]
Y11	PM6	0.83	16.54	0.74	26.74	[2]
Y18	PM6	0.84	16.52	0.76	25.7	[3]
L8-BO	PM6	0.87	18.32	0.82	25.72	[4]
L8-HD	PM6	0.88	17.39	0.79	25.08	[4]
N3	PFNT-Cl	0.853	18.10	0.799	26.56	[5]
N3	PFNT-F	0.842	17.53	0.800	26.03	[5]
BTP-4Cl	PM6	0.87	16.5	0.75	25.4	[6]
BTP-4F-12	PM6	0.86	16.2	0.76	25.3	[7]
BTP-eC9	PM6	0.84	17.8	0.81	26.2	[8]
BTP-eC11	PM6	0.85	16.9	0.77	25.7	[8]
BTP-4F-P2EH	PM6	0.88	18.22	0.80	25.85	[9]
AQx2	PM6	0.86	16.64	0.76	25.4	[10]
CH4	PM6	0.888	16.49	0.717	26.11	[11]
CH6	PM6	0.875	18.33	0.784	26.62	[11]
CH-6F	PM6	0.872	16.77	0.7599	25.31	[12]
CH-4Cl	PM6	0.872	17.72	0.7668	26.50	[12]
CH-6Cl	PM6	0.866	17.22	0.7628	26.07	[12]
BTP-C9-N4F	PM6	0.85	17.0	0.76	26.3	[13]
BTP-S8	PM6	0.852	17.33	0.7545	26.96	[14]
BTP-S9	PM6	0.846	17.56	0.7844	26.47	[14]
BTP-T-3Cl	PM6	0.893	17.61	0.7579	26.02	[15]
Qx-1	PM6	0.911	17.9	0.755	26.1	[16]
Qx-2	PM6	0.934	18.2	0.737	26.5	[16]

[1]   J. Yuan, Y. Zhang, L. Zhou, G. Zhang, H.-L. Yip, T.-K. Lau, X. Lu, C. Zhu, H. Peng, P. A. Johnson, M. Leclerc, Y. Cao, J. Ulanski, Y. Li and Y. Zou, *Joule*, 2019, 3, 1140-1151.

[2]   S. Liu, J. Yuan, W. Deng, M. Luo, Y. Xie, Q. Liang, Y. Zou, Z. He, H. Wu and Y. Cao, *Nat.*

Photonics, 2020, 14, 300-305.

[3] C. Zhu, J. Yuan, F. Cai, L. Meng, H. Zhang, H. Chen, J. Li, B. Qiu, H. Peng, S. Chen, Y. Hu, C. Yang, F. Gao, Y. Zou and Y. Li, *Energy Environ. Sci.*, 2020, 13, 2459-2466.

[4] H. Liu, T. Dai, J. Zhou, H. Wang, Q. Guo, Q. Guo and E. Zhou, *Nano Res.*, 2023, DOI: 10.1007/s12274-023-5693-z.

[5] S. Li, Q. Fu, L. Meng, X. Wan, L. Ding, G. Lu, G. Lu, Z. Yao, C. Li and Y. Chen, *Angew. Chem., Int. Ed.*, 2022, 61, e202207397.

[6] Y. Cui, H. Yao, J. Zhang, T. Zhang, Y. Wang, L. Hong, K. Xian, B. Xu, S. Zhang, J. Peng, Z. Wei, F. Gao and J. Hou, *Nat. Commun.*, 2019, 10, 2515.

[7] X. Ma, J. Wang, J. Gao, Z. Hu, C. Xu, X. Zhang and F. Zhang, Adv. Energy Mater, 2020, 10, 2001404.

[8] Y. Cui, H. Yao, J. Zhang, K. Xian, T. Zhang, L. Hong, Y. Wang, Y. Xu, K. Ma, C. An, C. He, Z. Wei, F. Gao and J. Hou, *Adv. Mater.*, 2020, 32, 1908205.

[9] J. Zhang, F. Bai, I. Angun, X. Xu, S. Luo, C. Li, G. Chai, H. Yu, Y. Chen, H. Hu, Z. Ma, H. Ade and H. Yan, *Adv. Energy Mater.*, 2021, 11, 2102596.

[10] Z. Zhou, W. Liu, G. Zhou, M. Zhang, D. Qian, J. Zhang, S. Chen, S. Xu, C. Yang, F. Gao, H. Zhu, F. Liu and X. Zhu, *Adv. Mater.*, 2019, 32, 1906324.

[11] H. Chen, H. Liang, Z. Guo, Y. Zhu, Z. Zhang, Z. Li, X. Cao, H. Wang, W. Feng, Y. Zou, L. Meng, X. Xu, B. Kan, C. Li, Z. Yao, X. Wan, Z. Ma and Y. Chen, *Angew. Chem., Int. Ed. Engl.*, 2022, 61, e202209580.

[12] Y. Zou, H. Chen, X. Bi, X. Xu, H. Wang, M. Lin, Z. Ma, M. Zhang, C. Li, X. Wan, G. Long, Y. Zhao and Y. Chen, *Energy Environ. Sci.*, 2022, 15, 4000.

[13] Y. Shi, J. Pan, J. Yu, J. Zhang, F. Gao, K. Lu and Z. Wei, Solar RRL, 2021, 5, 2100008.

[14] S. Li, L. Zhan, N. Yao, X. Xia, Z. Chen, W. Yang, C. He, L. Zuo, M. Shi, H. Zhu, X. Lu, F. Zhang and H. Chen, *Nat. Commun.*, 2021, 12, 4627.

[15] Y. Pan, X. Zheng, J. Guo, Z. Chen, S. Li, C. He, S. Ye, X. Xia, S. Wang, X. Lu, H. Zhu, J. Min, L. Zuo, M. Shi and H. Chen, *Adv. Funct. Mater.*, 2021, 32, 2108614.

[16] Y. Shi, Y. Chang, K. Lu, Z. Chen, J. Zhang, Y. Yan, D. Qiu, Y. Liu, M. A. Adil, W. Ma, X. Hao, L. Zhu and Z. Wei, *Nat. Commun.*, 2022, 13, 3256.

Table S11 Absorption coefficient of Qx-BO-1, Qx-BO-2 and Qx-BO-3.

	Qx-BO-1	Qx-BO-2	Qx-BO-3
ε-film (cm^{-1})	1.03×10^5	1.12×10^5	1.35×10^5
ε-sol (M^{-1}cm^{-1})	8.99×10^4	9.46×10^4	9.74×10^4

Table S12 Elemental analysis of Qx-BO-1, Qx-BO-2 and Qx-BO-3.

	C	H	N	S
Qx-BO-1(Cal.)	73.24	6.73	6.45	7.38
Qx-BO-1(Found)	73.25	6.75	6.46	7.36
Qx-BO-2(Cal.)	73.32	6.62	6.45	7.39
Qx-BO-2(Found)	73.19	6.61	6.30	7.33
Qx-BO-3(Cal.)	71.18	6.86	7.06	8.08
Qx-BO-3(Found)	71.18	6.91	7.04	8.06